Predicting the response of a submillimeter bolometer to cosmic rays

Adam L. Woodcraft, Rashmi V. Sudiwala, Peter A. R. Ade, Matthew J. Griffin, Elley Wakui, Ravinder S. Bhatia, Andrew E. Lange, James J. Bock, Anthony D. Turner, Minhee H. Yun, and Jeffrey W. Beeman

Bolometers designed to detect submillimeter radiation also respond to cosmic, gamma, and x rays. Because detectors cannot be fully shielded from such energy sources, it is necessary to understand the effect of a photon or cosmic-ray particle being absorbed. The resulting signal (known as a glitch) can then be removed from raw data. We present measurements using an Americium-241 gamma radiation source to irradiate a prototype bolometer for the High Frequency Instrument in the Planck Surveyor satellite. Our measurements showed no variation in response depending on where the radiation was absorbed, demonstrating that the bolometer absorber and thermistor thermalize quickly. The bolometer has previously been fully characterized both electrically and optically. We find that using optically measured time constants underestimates the time taken for the detector to recover from a radiation absorption event. However, a full thermal model for the bolometer, with parameters taken from electrical and optical measurements, provides accurate time constants. Slight deviations from the model were seen at high energies; these can be accounted for by use of an extended model.

OCIS codes: 040.0040, 040.3060, 040.7480.

1. Introduction

Bolometers are currently the best choice for sensitive direct detection of radiation at wavelengths between 200 μm and 2 mm (e.g., Refs. 1 and 2). Because a bolometer operates by measuring the heating due to absorbed energy, it is sensitive to any type of energy reaching the absorber. In most applications, filters are used to restrict the incident radiation to the wavelength range of interest. However, although filtering can provide extremely high rejection for most wavelengths,[3] it will not prevent cosmic, gamma, and x rays from reaching a bolometer.

Fortunately, such events do not present a continuous flux, but manifest themselves as sudden signal pulses, as a photon or cosmic-ray particle is absorbed, causing a rapid rise in temperature. Because it is not practical to prevent these events from occurring, it is necessary to understand their behavior so that they can be removed from raw data during analysis, in a process known as deglitching. This is particularly important when a bolometer is operated in a relatively high cosmic-ray flux such as is found on the Earth near the poles, or in space.

The conventional approach is to measure similar events and observe the behavior of the bolometer. We suggest an alternative approach: to use electrical and optical measurements on the bolometer to develop a model for the thermal properties, and use this to predict the behavior.

In this paper we examine the application of both approaches on a well-characterized semiconductor bolometer and compare the measured results with the model predictions. Bolometers similar to this are currently used for astronomy with ground- and

A. L. Woodcraft (adam.woodcraft@physics.org), R. V. Sudiwala, P. A. R. Ade, and M. J. Griffin are with the Department of Physics and Astronomy, University of Wales, Cardiff, P.O. Box 913, Cardiff CF24 3YB, United Kingdom. E. Wakui is with the Department of Physics, Queen Mary and Westfield College, Mile End Road, London E1 4NS, United Kingdom. R. S. Bhatia and A. E. Lange are with the California Institute of Technology, Mail Stop 59-33, Pasadena, California 91125. J. J. Bock, A. D. Turner, and M. H. Yun are with the Jet Propulsion Laboratory, California Institute of Technology, Pasadena, California 91109. J. W. Beeman is with the Lawrence Berkeley National Laboratory, Berkeley, California 94720.

Received 16 January 2003; revised manuscript received 9 May 2003.

0003-6935/03/255009-08$15.00/0

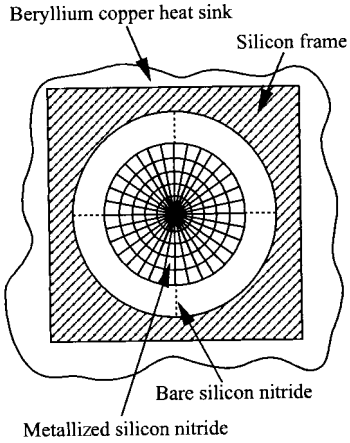

Fig. 1. Schematic diagram of the bolometer construction.

balloon-based telescopes and for satellite missions under development.

2. Measurements

All measurements described here were made on a prototype bolometer for the High Frequency Instrument (HFI)[4] on the Planck Surveyor cosmic microwave background imaging satellite[5] that is due to launch in 2007. It is a composite spider-web device,[6] contained in an integrating cavity within a lighttight module. The absorber consists of a 3.4-mm-diameter free-standing gold metallized silicon nitride mesh with 425-μm grid spacing. The temperature sensor is a neutron transmutation-doped[7,8] germanium thermistor chip, indium bump bonded to the center of the mesh.[6] A silicon frame, epoxied to a beryllium copper heat sink, supports the mesh by several unmetallized silicon nitride legs; see Fig. 1. The bolometer is designed to operate at a temperature of 100 mK. It should be noted that the optical time constant of this bolometer is significantly shorter than will be used for the flight HFI bolometers.

The measurements were carried out in an adiabatic demagnetization refrigerator (ADR) with optical access. This ADR provides cooling to temperatures below 100 mK with good control over the optical radiation incident on the bolometer. To make measurements, a constant voltage bias is applied to the bolometer thermistor, in series with two 60-MΩ load resistors, providing an approximately constant current bias. The thermistor voltage is read out by use of a cold matched pair of IFN146 silicon JFET (junction field-effect transistor) source followers, coupled to a low-noise external amplifier.

A thorough electrical and optical characterization of the bolometer was carried out.[9] Further details of these measurements, and of the bolometer, the ADR, and the measurement systems are given in Ref. 9.

In this paper we describe the results of pulse measurements using an Americium-241 gamma-ray source placed outside the cryostat. This generates photons with an energy of approximately 60 keV, some of which reach the bolometer through the cryostat and are absorbed. To make measurements, a constant bias voltage was applied to the bolometer, and the thermistor voltage was measured as a function of time at a sample rate of 10 kHz. Measurements were carried out at several temperatures, with a range of bias voltages used at each temperature. The bias values cover the region in which we would expect to operate the bolometer in normal use. For these measurements, the cryostat was in the optically open configuration in which submillimeter radiation was allowed to reach the bolometer through a window and a set of filters.[9]

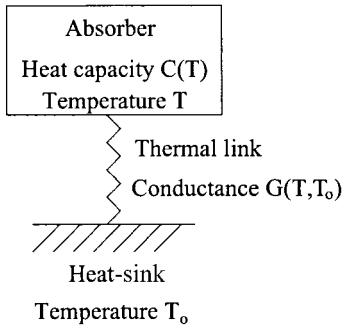

Fig. 2. Schematic of the simple bolometer model (the ideal bolometer).

We automatically extracted the pulses from the data by examining it for regions where the bolometer voltage deviated from the equilibrium value. We confirmed that all measured pulses were produced by the gamma source by taking measurements with the source removed. The variation of pulse behavior with the bolometer temperature demonstrates that the pulses are indeed due to energy absorbed in the bolometer and not in the readout electronics.

3. Characterization

A simplified model (the ideal bolometer) describes a bolometer as consisting of a thermistor mounted on an absorber, which is connected to a heat sink by a weak thermal link[10], see Fig. 2. It is usual to use a power law to describe the conductivity of the thermal link, resulting in an expression such as

$$G = G_{S0}T^{\beta} \tag{1}$$

for the conductance G as a function of temperature T, for some constant G_{S0}. (This expression is true only when the bolometer and heat sink are at the same temperature; if they are at different temperatures, the change in conductivity with temperature along the thermal link must be taken into account, resulting in a more complicated expression.[10])

In addition, it is necessary to determine the thermistor resistance as a function of temperature. For the bolometer described here, this dependence was found to be in good agreement with the Coulomb gap variable-range hopping equation[11]:

$$R(T) = R_0 \exp\sqrt{\frac{T_g}{T}}, \tag{2}$$

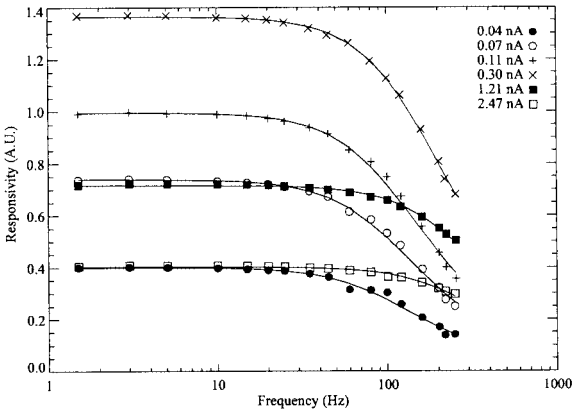

Fig. 3. Bolometer responsivity as a function of optical radiation modulation frequency for a heat-sink temperature of 100 mK and various bias currents. The curves show fits to the data for each bias current, assuming a single time constant. Note that the responsivity peaks as a function of bias[9] whereas the time constant decreases monotonically. Therefore, for a given responsivity, there are two time constants corresponding to bias values above and below the value at which the responsivity peaks. The y axis is plotted with arbitrary units.

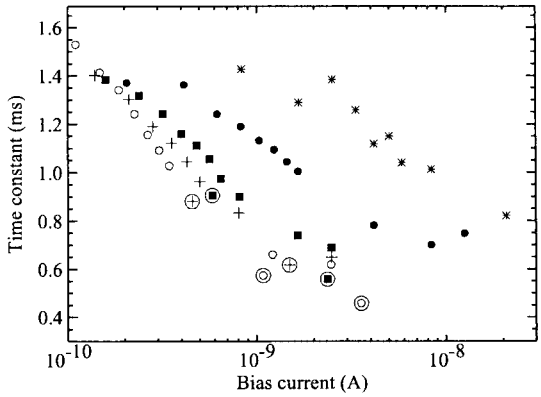

Fig. 4. Uncircled points show time constants obtained from measuring the response to modulated optical radiation as a function of bias current and heat-sink temperature. The temperatures are 100 mK (○), 110 mK (+), 120 mK (■), 150 mK (●) and 220 mK (*). Circled points show the time constant from gamma photon absorption events, in the limit of zero energy pulses, with temperature represented by the same symbols.

where R is the resistance at temperature T, and T_g and R_0 are constants that depend on the thermistor properties.

The parameters R_0 and T_g can be determined by measuring the thermistor resistance in the limit of zero bias for a range of heat-sink temperatures. Once these are determined, G_{S0} and β can be calculated by measuring the absorber temperature as a function of dissipated electrical power in the thermistor.[9]

The results from these measurements were in good agreement with the ideal model[9]; the behavior of the bolometer could be described accurately over a wide temperature range by use of constant values of the parameters G_{S0}, β, R_0, and T_g.

Similar measurements were carried out with the bolometer exposed to a known radiation load (a 300 K blackbody); these were used to obtain the absorbed power Q.

To model pulse events, it is also necessary to understand the dynamic behavior of the bolometer. This can be done by measuring the response to a modulated radiation source. Measurements were made for radiation modulated at frequencies between 1.5 and 250 Hz, at a range of heat-sink temperatures and thermistor bias levels.[9]

The result for each temperature and bias could be fitted well assuming a single time constant. An example is shown in Fig. 3. The time constants as a function of temperature and bias are shown in Fig. 4.

The absorber heat capacity can be calculated by multiplying the time constants by the effective thermal conductance[10], obtained from the modeled conductance values (G_{S0} and β). We assume that the heat capacity of the thermal link itself is negligible; this assumption is justified by the fact that the thermal link constitutes a small fraction of the thermal mass of the bolometer.

As shown in Ref. 9, a simple power law could be used to describe the heat capacity as a function of temperature. However, discrepancies were seen below 120 mK, with different values being obtained for the heat capacity for the same absorber temperature but different heat-sink temperatures.

We cannot explain these results, although they may be related to nonideal effects in the thermistor.[9] Fitting to the data above 120 mK, and describing the absorber heat capacity as

$$C = C_0 T^{\beta_c}, \tag{3}$$

we can model the dynamic behavior of the bolometer using C_0, β_c, and the parameters G_{S0}, β, R_0, T_g described above.

We show in Section 5 that the discrepancies below 120 mK do not affect the accuracy of the model. In any case, the absorber temperature will be approximately 120 mK or higher when the bolometer is in normal use.

4. Results

Overall, we obtained approximately 100 pulses, with data taken at 13 combinations of heat-sink temperature and bias voltage. For each temperature and bias, a range of pulse energies was detected. Generally, a number of pulses were seen with similar energies, with the remainder being scattered at lower energies. These latter pulses presumably result from incomplete absorption of the energy.

Figure 5 shows some of the measured pulses. The rise time is barely resolved. The fall times were fitted assuming an exponential decay. All pulses could be fitted well in this manner.

For a given bias current and heat-sink temperature, similar time constants are seen for any given pulse height. This shows that the bolometer is well constructed, with a highly conducting absorber, in good thermal contact with the thermistor. If this

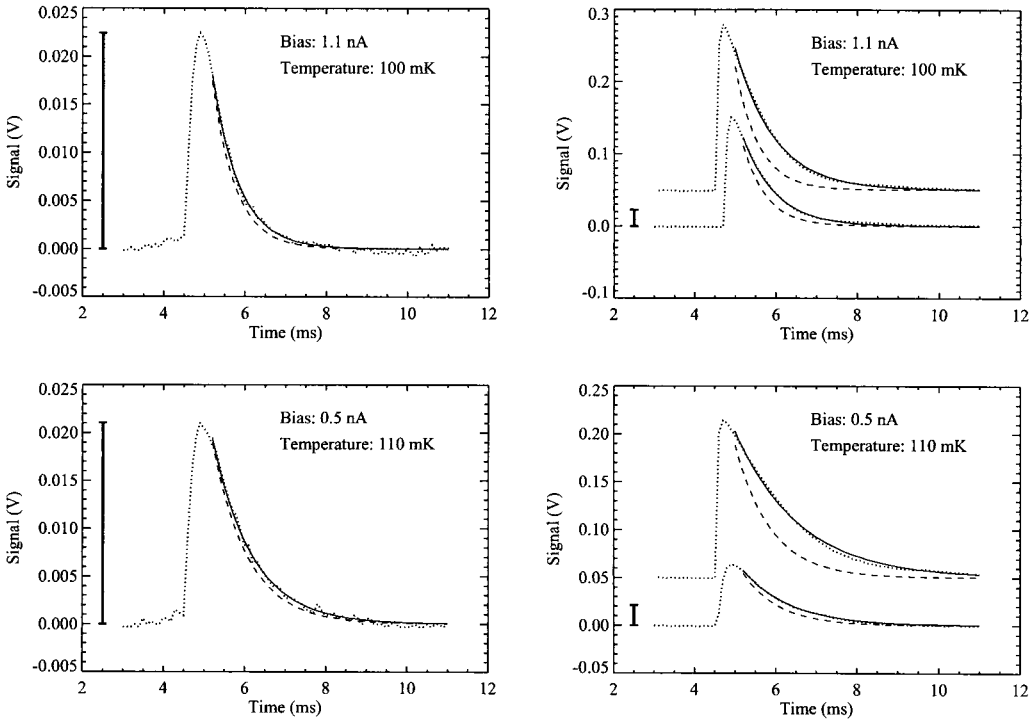

Fig. 5. Pulses in bolometer voltage following absorption of a gamma-ray photon (dotted curves). Solid curves show simple exponential fits to the data. Dashed curves show an exponential decay in which the time constant of the exponential fits in the limit of zero pulse energy is used; the dashed curves therefore have the same time constant for a given bias and temperature. Where two pulses are shown in a single graph, the upper pulse is offset vertically and horizontally. Note the different y-axis scales; the scale bars at the left of each graph show the same temperature range for adjacent graphs.

was not the case, a range of time constants would be seen depending on where the photons were absorbed.

However, as shown in Fig. 6, the time constants vary considerably with pulse height. From this data, the time constant in the limit of zero pulse height can be calculated. This is compared with the optical time constants in Fig. 4; the agreement is good.

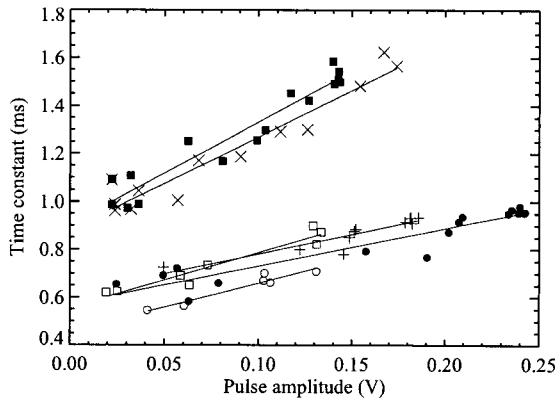

Fig. 6. Time constant of voltage pulses as a function of the pulse peak amplitude for various heat-sink temperatures and bias currents. The combinations of temperature and bias, respectively, are 100 mK, 1.1 nA (●), 100 mK, 3.6 nA (○), 110 mK, 0.5 nA (×), 110 mK, 1.5 nA (+), 120 mK (□), 2.4 nA, 120 mK, 0.6 nA (■). The solid curves are linear fits to each set of data. The apparent grouping of the time constants into two sets reflects a similar grouping of the chosen bias values.

It is not surprising that the time constants increase at larger pulse heights. During optical measurements, the absorber temperature changes are small: for example, 2 mK at a 100-mK heat-sink temperature. The larger pulses correspond to much larger temperature changes than this; the variation of heat capacity and thermal conductance with temperature will then alter the time constant. This behavior has been seen in models of similar systems. It should also be noted that the voltage should not exactly follow an exponential decay because the resistance is not a linear function of temperature.

It is clear that use of the optical time constants can seriously underestimate the amount of time taken to recover from a pulse. This is shown in Fig. 5 where the predicted behavior with the zero pulse height time constant is shown (as dashed curves). To predict the response to a pulse of arbitrary energy requires a more sophisticated analysis.

5. Modeling

The temperature evolution of the bolometer absorber was modeled numerically. The parameters used are shown in Table 1; G_{S0}, β, C_0, β_c, Q, R_0, and T_g are taken from the characterization described in Section 3. The model calculates the change in temperature over a given time interval by using the absorber heat

Table 1. Parameters Used in the Pulse Modeling Along with the Values Used[a]

Property	Parameter	Value
Weak link thermal conductance	G_{S0}	1500 pW K^{-1}
	β	1
Absorber heat capacity	C_0	2.9 pJ K^{-1}
	β_c	1.2
Absorbed optical power	Q	0.35 pW
Heat-sink temperature	T_0	
Applied bias voltage	V_{bias}	
Load resistance	R_L	120 MΩ
Thermistor calibration	R_0	143 Ω
	T_g	13.3 K

[a]Values for T_0 and V_{bias} are not given because they vary between pulses.

capacity and the net power gained and lost by the absorber.

Power is gained from absorbed optical radiation Q and heating that is due to the thermistor bias,

$$P_{elec} = \left(\frac{V_{bias}}{R_L + R}\right)^2 R , \quad (4)$$

and lost because conduction to the heat sink:

$$P_{link} = \frac{G_{S0}}{\beta + 1}(T^{\beta+1} - T_0{}^{\beta+1}) \quad (5)$$

(radiative losses are negligible at these temperatures). The change in temperature ΔT over a time interval Δt is then

$$\Delta T = \frac{(P_{elec} + Q - P_{link})}{C_0 T^{\beta_c}} \Delta t . \quad (6)$$

To compare the model with the experimental data it is necessary to calculate the absorber temperature from the thermistor resistance by use of Eq. (2). Unfortunately, during our measurements, only the deviation in thermistor voltage from the equilibrium value was measured. Calculating the resistance requires the absolute voltage to be known. However, it is possible to determine this voltage indirectly. The equilibrium voltage as a function of bias current is known from previous voltage–current measurements.[9] To reconstruct the absolute voltage we can use the measured voltage deviations, along with a value for the equilibrium voltage for the same heat-sink temperature and bias as the pulse measurement.

The only adjustable parameter in the model corresponds to the variation in absorbed photon energy. This is accounted for by starting the model with the measured temperature at the peak of the pulse. However, the procedure described above to recover the equilibrium thermistor voltage forces the modeled equilibrium absorber temperature to agree with the measured value. If the actual equilibrium thermistor voltage was known, it would probably be necessary to also include a fitting parameter to allow small adjustments to ensure this agreement. One way to do this would be to vary the value used for the absorbed optical power Q.

Figure 7 shows some pulses along with the modeled values. The accuracy of the numerical computations was confirmed by changing the temperature step used in Eq. (6). It can be seen that the model is highly successful, producing good fits over the full range of temperature and bias.

The model can also be used to calculate the energy for each pulse E by integrating the absorber heat capacity C over the change in temperature:

$$E = \int_{T_0}^{T_i} C(T)\mathrm{d}T = \frac{C_0}{\beta_c + 1}(T_i{}^{\beta_c+1} - T_0{}^{\beta_c+1}) , \quad (7)$$

where T_i is the initial pulse energy. The results are shown in Fig. 8. The maximum energies measured are close to the expected value of 60 keV; this provides further evidence for the validity of our thermal model. There is an apparent dependence of energy on absorber temperature at the lower temperatures; this is unlikely to be real and may be related to the discrepancies seen in the heat capacity below 120 mK.

An obvious question to ask is whether the model will work for higher absorbed energies than used in this experiment. One way to investigate this is to see if there is any evidence of the model breaking down. Figure 9 shows high- and low-energy pulses (taken at the same bias and heat-sink temperature) over a fixed absorber temperature range. This range includes the whole of the low-energy pulses, but covers only a small section near the tail of the high-energy pulses. The time constants are significantly different, approximately 1 and 2 ms for the low- and high-energy pulses, respectively. (Note that the overall fit to the high-energy pulse is good, apart from the tail region). Therefore there is a dependence on the thermal history of the bolometer. This is not something that can be explained by the simple model, which has only one independent variable—the absorber temperature.

A simple extended model to explain this behavior is to assume that the bolometer is connected to the heat sink by a component with a relatively large heat capacity (see Fig. 10). For low-energy pulses (and optically modulated power) this will remain at a nearly constant temperature. However, for high-energy pulses it will have time to warm up and thus reduce the temperature gradient across the thermal link to the absorber, resulting in a slower thermal decay. Physically, this could correspond to the silicon support frame (Fig. 1).

Determining the parameters for this model is not straightforward. Electrical characterization measurements actually measure the two thermal links in series. Because our measurements were consistent with a simple power law, this suggests that both thermal links have a similar temperature dependence.

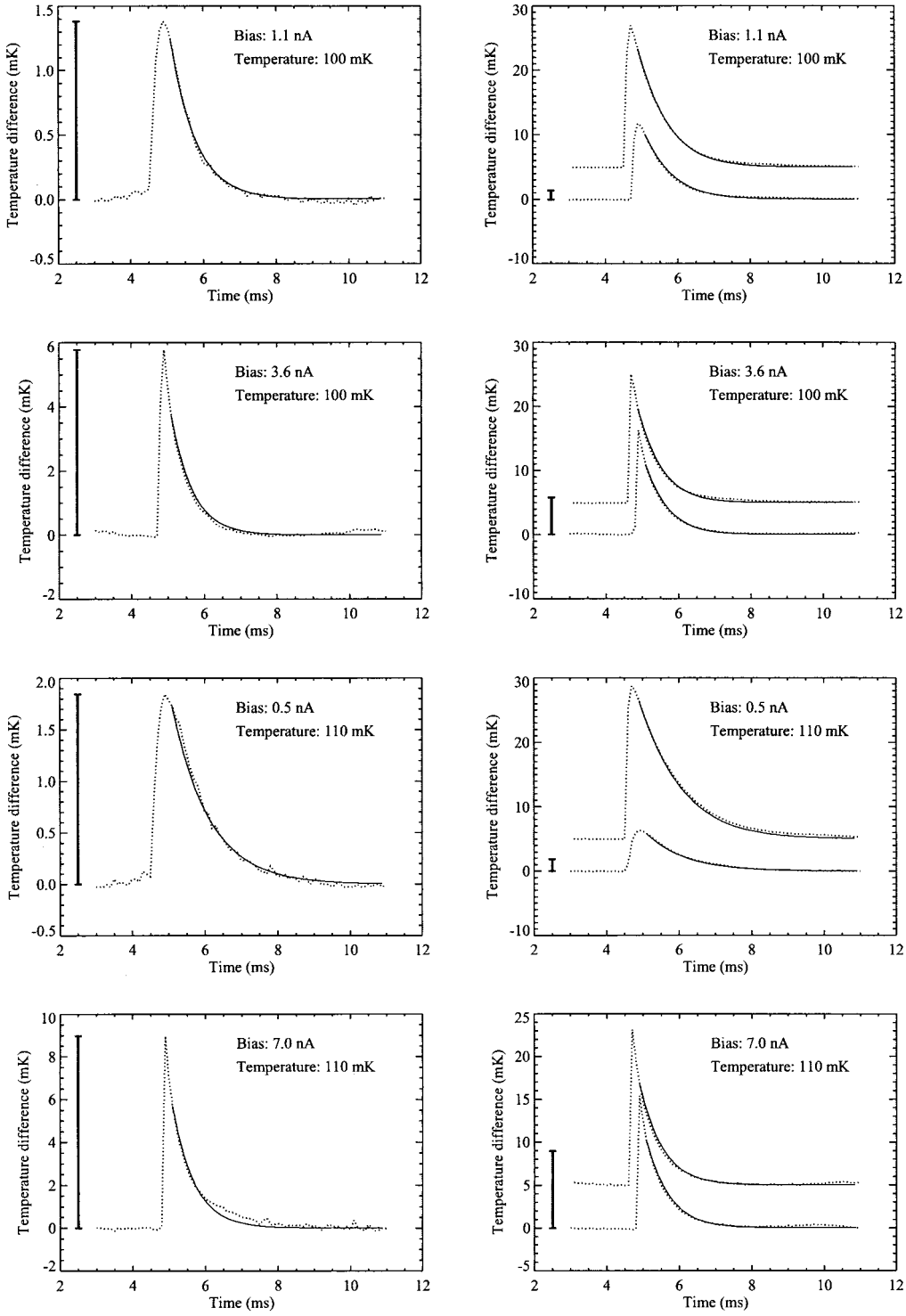

Fig. 7. Pulses at various heat-sink temperatures and bolometer bias currents. The difference between the absorber temperature and its equilibrium temperature is plotted. Dotted curves show the measured data, and the solid curves show the results from the simple (single heat capacity) model. Note that these are not fits to the pulses, but thermal simulation curves based on only one adjustable parameter—the chosen initial temperature, taken from the measured data (although as described in the text, the model equilibrium temperature is effectively constrained to agree with the data). Where two pulses are shown in a single graph, the upper pulse is offset vertically and horizontally. Note the large variation in y-axis scales; the scale bars at the left of each graph show the same temperature range for adjacent graphs.

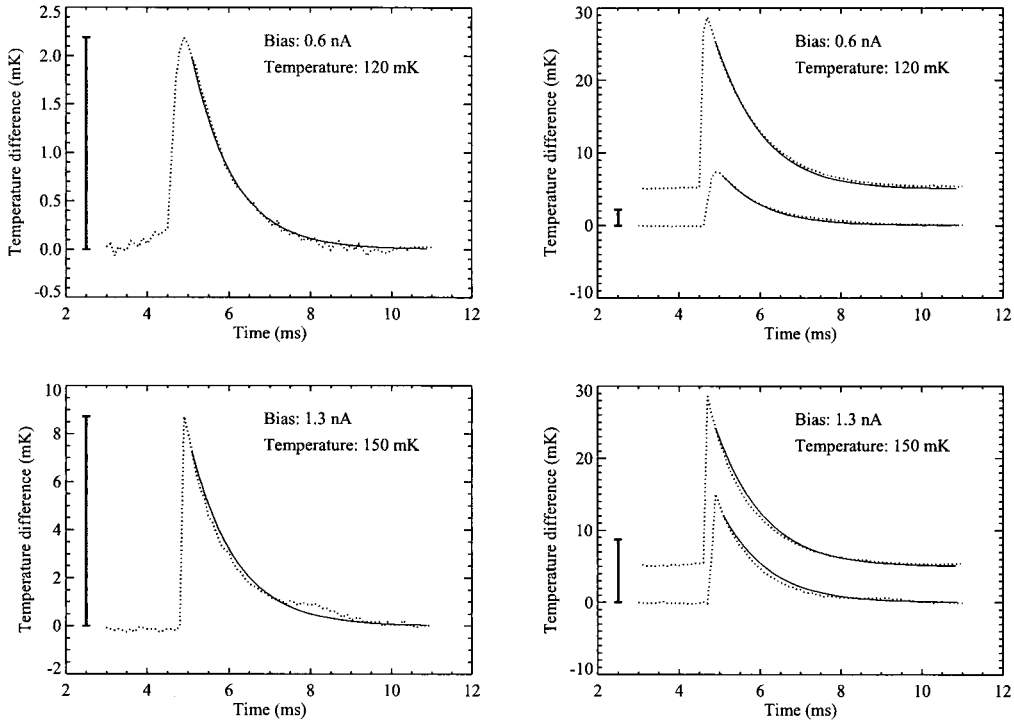

Fig. 7. Continued

However, this still leaves the prefactor for the conductance of each thermal link (G_{S0}) to be determined, as well as the heat capacity of the second component as a function of temperature. We do not have sufficient data to determine these parameters with any accuracy. However, making the arbitrary assumption that the second heat capacity has the same temperature variation as the absorber, we found values for the remaining parameters that produce good fits to the data in Fig. 9. This suggests that the extended model is a plausible explanation for the observed behavior. The data set used in Fig. 9 was selected because it shows this nonideal behavior most clearly. Use of the same parameters for data sets at other heat-sink temperatures and biases produces fits that are in approximate agreement.

This effect, although small, is potentially significant. It increases the recovery time from an event over that predicted by the simple model, and the increase should become larger with increasing pulse energy. However, the bolometers that will fly on HFI will have significantly longer primary time con-

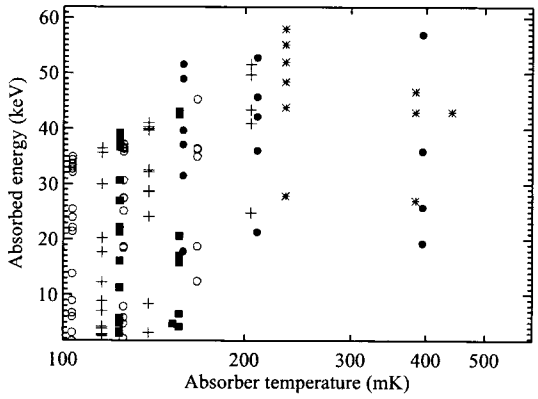

Fig. 8. Calculated absorbed energy from each event as a function of absorber equilibrium temperature. The symbols are the same as in Fig. 4.

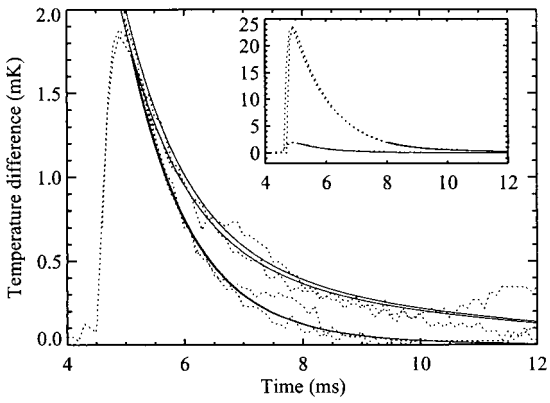

Fig. 9. Comparison of the absorber temperature variation for two low-energy pulses with the low-temperature section of two high-energy pulses (dotted curves). The high-energy pulses are offset along the x-axis for better comparison with the low-energy pulses. The solid curves show fits to the data with a two heat capacity model (see text). The inset shows the same information, with an expanded y axis to show the full height of the high-energy pulse. For comparison, the fits (solid curves) are limited to the temperature region shown in the main graph. The measurements were taken at a bias of 0.5 nA and a heat-sink temperature of 110 mK.

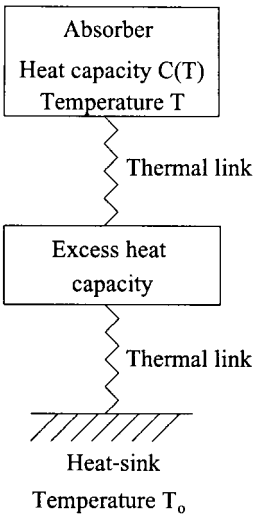

Fig. 10. Schematic of the extended (two heat capacity) bolometer model.

stants than the bolometer discussed here (4–8 ms, depending on optical frequency, matching the modulation time for astrophysical signals). This increase in time constant will reduce the impact of an effect of this size.

Although the effect was not detected during electrical and optical characterization, it could presumably be measured electrically by monitoring the transient bolometer voltage following a sudden large change in bias.

We conclude that the model can be used with caution to predict the response to higher absorbed energies. However, experimental results with higher energies would be useful to confirm this.

6. Conclusions

We have measured the effects of the absorption of gamma-ray photons by a semiconductor bolometer, a prototype for HFI.[4] The observed thermal time constants did not appear to vary with absorption position, suggesting that the bolometer absorber and thermistor thermalize quickly, as is desirable.

Small deviations from the model were seen at high pulse energies. These can be explained qualitatively by an extension to the model.

We have shown that it is possible to use standard electrical and optical characterization measurements to make accurate predictions of the response to pulse events of different energies. The simpler method which uses time constants obtained from optical measurements was accurate for low-energy pulses but underestimated the recovery time from higher-energy pulses.

Such predictions are important in designing data reduction routines to identify and remove cosmic-ray events from raw data (deglitching). This could consist of merely removing data known to be contaminated by the effect of a glitch, or possibly of using the model to compensate for the glitch and reconstruct the behavior in its absence.

These results could also be used to examine what portion of the data from an instrument such as HFI is likely to be affected by cosmic-ray events. However, such a calculation requires both a knowledge of the cosmic-ray flux as a function of energy at the location of the detectors within the spacecraft and a detailed understanding of the interaction of cosmic rays with the bolometer absorber and is thus outside the scope of this paper.

To summarize, our results extend the range of behavior in which the bolometer has been shown to be in good agreement with the ideal bolometer model. The more closely a bolometer agrees with the model, the easier it is to understand its behavior and to use it to obtain accurate measurements.

References

1. P. L. Richards, "Bolometers for infrared and millimeter waves," J. Appl. Phys. **76,** 1–24 (1994).
2. M. J. Griffin, "Bolometers for far-infrared and submillimetre astronomy," Nucl. Instrum. Methods Phys. Res. A **444,** 397–403 (2000).
3. C. Lee, P. A. R. Ade, and C. V. Haynes, "Self supporting filters for compact focal plane designs," in *Proceedings of the 30th ESLAB Symposium: Submillimetre and Far-Infrared Space Instrumentation* (European Space Agency, Noordwijk, The Netherlands, 1996), SP. 388, pp. 81–83.
4. J. M. Lamarre, P. A. R. Ade, A. Benoît, P. de Bernardis, J. Bock, F. Bouchet, T. Bradshaw, J. Charra, S. Church, F. Couchot, J. Delabrouille, G. Efstathiou, M. Giard, Y. Giraud-Héraud, R. Gispert, M. Griffin, A. Lange, A. Murphy, F. Pajot, J. L. Puget, and I. Ristorcelli, "The high frequency instrument of Planck: design and performances," Astro. Lett. Commun. **37,** 161–170 (2000).
5. N. Mandolesi and M. Villa, "FIRST/Planck mission," in V. Piuri and M. Savino, eds., *ICMT/99: Proceedings of the 16th IEEE Instrumentation and Measurement Technology Conference* (Institute of Electrical and Electronics Engineers, Piscataway, N.J., 1999), Vol. 2, pp. 975–980.
6. M. Yun, J. Beeman, R. Bhatia, J. Bock, W. Holmes, L. Husted, T. Koch, J. Mulder, A. Lange, A. Turner, and L. Wild, "Bolometric detectors for the Planck Surveyor," in *Millimeter and Submillimeter Detectors for Astronomy*, T. G. Phillips and J. Zmuidzinas, eds., SPIE **4855,** 136–147 (2002).
7. E. E. Haller, "Advanced far-infrared detectors," Infrared Phys. Technol. **35,** 127–146 (1994).
8. E. E. Haller, K. M. Itoh, and J. W. Beeman, "Neutron transmutation doped (NTD) germanium thermistors for sub-mm bolometer applications," in *Proceedings of the 30th ESLAB Symposium: Submillimetre and Far-Infrared Space Instrumentation* (European Space Agency, Noordwijk, The Netherlands, 1996), SP. 388, pp. 115–118.
9. A. L. Woodcraft, R. V. Sudiwala, M. J. Griffin, E. Wakui, B. Maffei, C. E. Tucker, C. V. Haynes, F. Gannaway, P. A. R. Ade, J. J. Bock, A. D. Turner, S. Sethuraman, and J. W. Beeman, "High precision characterisation of semiconductor bolometers," Int. J. Infrared Millim. Waves **23,** 575–595 (2002).
10. R. V. Sudiwala, M. J. Griffin, and A. L. Woodcraft, "Thermal modelling and characterisation of semiconductor bolometers," Int. J. Infrared Millim. Waves **23,** 545–573 (2002).
11. A. L. Efros and B. I. Shklovskii, "Coulomb gap and low temperature conductivity of disordered systems," J. Phys. C **8,** L49–L51 (1975).